

Development of a Fe–He interatomic potential based on electronic structure calculations

T. Seletskaja^a, Yu.N. Osetskiy^b, R.E. Stoller^{a,*}, G.M. Stocks^a

^a Materials Science and Technology Division, Oak Ridge National Laboratory, Bldg. 4500S, MS-6138,
P.O. Box 2008, Oak Ridge, TN 37831-6138, United States

^b Computer Science and Mathematics Division, Oak Ridge National Laboratory, Oak Ridge, TN 37831-6138, United States

Abstract

A new empirical Fe–He potential has been developed by fitting results obtained from first-principles calculations. Both the formation and relaxation energies of single He defects and small He clusters were accounted for in the fitting process. The new potential consists of a repulsive pair-potential term and a three-body interaction term, and was applied in combination with three commonly used iron interatomic potentials, and a potential describing the behavior of helium in vacuum. As an application of the new potential, the stability of He–vacancy clusters at zero temperature was evaluated. The calculated results were similar for all three Fe potentials, and the new potentials provide results that are more consistent with *ab initio* calculations than those obtained from previous Fe–He potentials.

© 2007 Elsevier B.V. All rights reserved.

1. Introduction

Helium is produced in neutron-irradiated metals by (n, α) transmutation reactions and plays a significant role in microstructural evolution and mechanical properties degradation [1,2]. However, helium's high mobility via an interstitial migration mechanism and its strong binding with vacancies make it difficult to experimentally assess its atomistic behavior. First-principles electronic structure calculations provide the most direct approach to obtaining this information; but, such calculations cannot be carried out on the time and size scales needed to simulate important issues such as the evolution of

helium-vacancy clusters. Applying *ab initio* data to construct an empirical potential for use in classical molecular dynamics seems to be the most practical approach currently available to study He behavior in metals on the desired scale.

A previous effort led to the construction of a Fe–He empirical potential by Wilson [3] in the late 1960s. The potential was defined as a pair-wise interaction energy for a Fe–He⁰ dimer which ignored the bulk properties of the metal matrix, making it inappropriate for simulating the energy and dynamic properties of He defects in iron. Electronic structure calculations [4,5] have demonstrated that Wilson's potential predicts the wrong site preference for the He interstitial defect and significantly overestimates the binding energy of a single He atom to a vacancy. A pair-potential model is not generally suitable for Fe–He interactions

* Corresponding author. Tel.: +1 865 5767886; fax: +1 865 2413650.

E-mail address: rkn@ornl.gov (R.E. Stoller).

because a pair potential cannot accurately describe both the forces and formation energies of He defects [6]. A Fe–He interaction arises from electronic hybridization between Fe d- and He s-electrons which is strong enough to change the magnetic moment of neighboring He iron atoms [4].

In previous work [7], a Fe–He empirical potential was fitted to first-principles results with high accuracy. The potential consisted of a pair potential and an embedding function. The latter modified the He–He interaction and made the potential unsuitable for problems involving a low density He gas such as would exist inside a cavity in iron. Here a different model is developed that does not have this deficiency. The form of the potential was inferred from the electronic structure calculations. The potential was used to study He–vacancy cluster stability at zero temperature using the classical molecular statics (MS) technique.

2. Methodology

The following functional form was chosen for the total energy of a Fe–He system consisting of I_{Fe} iron atoms and I_{He} helium atoms:

$$E = \sum_{i \in I_{\text{Fe}}} \Phi_{\text{Fe}}(\rho_i) + \sum_{\substack{i \in I_{\text{Fe}} \\ j \neq i, j \in I_{\text{Fe}}}} \varphi_{\text{FeFe}}(r_{ij}) + \sum_{\substack{i \in I_{\text{He}} \\ j \in I_{\text{He}}}} \varphi_{\text{HeHe}}(r_{ij}) \\ + \sum_{\substack{i \in I_{\text{He}} \\ j \neq i, j \in I_{\text{Fe}}}} \varphi_{\text{FeHe}}(r_{ij}) + \sum_{\substack{i \in I_{\text{He}} \\ j \in I_{\text{Fe}} \\ k \neq j, k \in I_{\text{Fe}}}} Y_{\text{He}}(r_{ij}, r_{ik}, \Theta_{jik}), \quad (1)$$

where the first two terms describe the Fe–Fe interaction; the third and the fourth terms are He–He and a Fe–He pair potentials, respectively; and the fifth term introduces a Fe–He three-body interaction. Three potentials describing the Fe–Fe interaction were assessed in this work: one by Finnis and Sinclair [8], and two by Ackland and co-workers [9,10]. For convenience, the 1997 potential by Ackland et al. [9] will be referred to as Ackland-I and the 2004 potential [10] based on the work of Mendeleev et al. [11] as Ackland-II. Each of the Fe potentials include a many-body term which depends on the atomic density ρ_i , and a repulsive pair potential which is a function of the interatomic distance r_{ij} . The pair potential of Aziz et al. [12] that describes He properties in vacuum was used for the He–He interaction term.

An empirical Fe–He potential consisting of a pair-potential term, $\varphi_{\text{FeHe}}(r_{ij})$ and a three-body

term, $Y_{\text{He}}(r_{ij}, r_{ik}, \Theta_{jik})$, was obtained by fitting the results of first-principles calculations. The calculations were performed using the Vienna *ab initio* simulation package (VASP) as described in previous publications [4,7]. The objective was to fit formation and relaxation energies of the single He defect and small He clusters. Interstitial He in both the octahedral and tetrahedral positions, and the substitutional He defect (He octa, He tetra and He sub) [4] were evaluated. He clustering behavior was investigated for both interstitial and vacancy-type defects. These included a He di-interstitial, and clusters with two and three He atoms located inside one vacancy (2He, 2He–vac and 3He–vac) [7].

The long-range part of the pair potential was first fit using a simple and relatively flexible mathematical form:

$$\varphi_{\text{FeHe}}(r_{ij}) = p_1 \left(1 - p_2 \left(\frac{r_{ij}}{p_3} - 1 \right) \right) e^{-p_4 \left(\frac{r_{ij}}{p_3} - 1 \right)} \cdot f_{\text{cut}}(r_{ij}), \quad (2)$$

where $f_{\text{cut}}(r_b, r_c, r_{ij})$ is a cutoff function whose first and second derivatives vanish when $r_{ij} = r_b$ and $r_{ij} = r_c$:

$$f_{\text{cut}}(r_{ij}) = (1-x)^3(1+3x+6x^2), \quad \text{where } x = \frac{r_{ij} - r_b}{r_c - r_b}. \quad (3)$$

For $r_{ij} < r_b$, $x = 0$ and for $r_{ij} > r_c$, $x = 1$. The function $\varphi_{\text{FeHe}}(r_{ij})$ has three fitting parameters (p_1 , p_2 , and p_4) since p_3 is simply a scaling factor.

Values for these parameters were obtained by a least-squares fitting procedure involving the three unrelaxed formation energies and forces, and seven relaxed formation energies for the Ackland-I [9] Fe matrix potential as described in [7]. Since the three-body interaction acts only over short distances in the interstitial region, the parameters of the pair potential were fitted to the formation energy of the He substitutional defect, and of 2 and 3 He atoms in a vacancy. The smallest Fe–He separation in these configurations is equal to 1.68 Å. The minimization of the sum of squared differences was performed by the conjugate-gradient method. However, since this procedure does not guarantee zero forces for the relaxed configurations, the potential was used to relax these configurations by classical MS in a 128-atom supercell as was done for the VASP calculations [4,9]. The parameters $\{p_i\}$ were varied and the relaxation repeated to obtain a

minimum sum of squared differences between *ab initio* and MS simulations.

This pair potential reproduced He behavior in vacuum, but strongly underestimated the formation energies of He interstitials. To fit the energies of the interstitial, we used an exponential function for interatomic distances less than 1.6 Å and a simple polynomial to smoothly join this function with the long-range part of the pair-potential. As a result, the pair-potential is written:

$$\varphi_{\text{FeHe}}(r_{ij}) = \begin{cases} \exp(b_1 + b_2x + b_3x^2 + b_4x^3 + b_5x^4), & r_{ij} < 1.6 \text{ \AA}, \\ a_1 + a_2x + a_3x^2 + a_4x^3 + a_5x^4 + a_6x^5, & 1.6 \text{ \AA} \leq r_{ij} < 2.2 \text{ \AA}, \\ \varphi(r_{ij}), & 2.2 \text{ \AA} \leq r_{ij} < 4.4 \text{ \AA}, \end{cases} \quad (4)$$

where $\varphi(r_{ij})$ is given by Eq. (2). The parameters of the potential are given in Table 1.

A three-body potential term was introduced to improve the fitting for the interstitial properties. It has the following form:

$$Y_{\text{He}}(r_{ij}, r_{ik}, \Theta_{jik}) = \sum_{\substack{j \in I_{\text{Fe}} \\ k \neq j, k \in I_{\text{Fe}}}} f^Y(r_{ij})f^Y(r_{ik})\cos^2(\Theta_{jik} - 0.44), \quad (5)$$

where the summation is performed over pairs of Fe neighbors of the He atom separated by the distances r_{ij} and r_{ik} . The functions $f^Y(r)$ represent the distance-dependence of the three-body potential and Θ_{jik} is the angle between the radius-vectors r_{ij} and r_{ik} drawn from the He atom as the center. To guarantee the preference for the tetrahedral site over the octahedral, the angle of 0.44 rad (the average angle formed by Fe–He vectors in the tetrahedral position minus $\pi/2$) is subtracted. The functions $f^Y(r)$ in Eq. (5) are given by Eq. (3), with the right-hand side multiplied by the parameter a^Y . Since hybridization between Fe and He atoms is weak, the three-body term provides only a small correction to the pair-potential. The fitting of a^Y was initiated with a value of zero and it was gradually increased until all the formation energies were fit. The values of a^Y and r_b^Y are 0.7 eV^{1/2} and 1.75 Å, respectively. The cutoff of the three-body energy, r_c^Y , was chosen to be 2.2 Å.

Table 1
Parameters for pair potential given by Eqs. (2) and (5)

$b_1 = -2.142600207811$	$a_1 = -285.7450302953, \text{ eV}$	$p_1 = 0.167753, \text{ eV}$
$b_2 = 32.965470333178, \text{ \AA}^{-1}$	$a_2 = 794.5913355517, \text{ eV, \AA}^{-1}$	$p_2 = 0.000000$
$b_3 = -52.893449935488, \text{ \AA}^{-2}$	$a_3 = -856.9376372455, \text{ eV, \AA}^{-2}$	$p_3 = 2.432258, \text{ \AA}$
$b_4 = 30.970079966695, \text{ \AA}^{-3}$	$a_4 = 452.5323035795, \text{ eV, \AA}^{-3}$	$p_4 = 3.727249$
$b_5 = -6.398785336260, \text{ \AA}^{-4}$	$a_5 = -117.6519447529, \text{ eV, \AA}^{-4}$	$r_b = 4.1, \text{ \AA}$
	$a_6 = 12.0878858024, \text{ eV, \AA}^{-5}$	$r_c = 4.4, \text{ \AA}$

Table 2
Results of fitting He defect formation energies (eV) in Fe

Defect	VASP	Fe potentials		
		Finnis–Sinclair	Ackland-I	Ackland-II
<i>Unrelaxed structures</i>				
He octa	6.37	6.40	6.40	6.55
He tetra	5.70	5.72	5.72	5.83
He sub	3.99	3.98	3.82	3.74
<i>Relaxed structures</i>				
He octa	4.60	4.74	4.70	4.57
He tetra	4.36	4.37	4.33	4.26
He _{i-mid}	4.42	4.40	4.37	4.29
He sub	3.73 ^a	3.82	3.70	3.75
He–He–vac	6.29 ^a	6.49	6.35	6.46
He–He–He–vac	9.09 ^a	9.39	9.23	9.37
He–He inter.	8.72 ^a	8.59	8.54	8.24

^a Values listed for VASP have been adjusted to account for the difference in vacancy or SIA formation energy predicted by VASP and the Ackland-I potential [7].

3. Results

The results of the fitting procedure for a single He defect and small He clusters are presented in Table 2. Note that the value of the He-substitutional formation energy listed for VASP is lower than the original value 4.08 eV reported in [4]. This is because the vacancy formation energy obtained with the Ackland-I potential is 0.35 eV lower than that from DFT calculations. Since the objective was to fit the Fe–He potential to the binding energy of a He atom with vacancy, the VASP value was adjusted for this difference in the comparison. An analogous adjustment was applied for the formation energy of all defects involving both He atoms and either vacancies or SIAs. It is clear that similar results are obtained for He defects when the Fe–He potential is used in combination any of the different Fe potentials. This is a natural result of using the same Fe–He potential. The small differences listed for the He defect formation energies in unrelaxed structures are the result of the different Fe potentials predicting slightly different equilibrium lattice parameters and vacancy formation energies. The relaxation of Fe atoms around a He defect depends on the stiffness of the Fe potential. Thus, the differences are slightly larger for relaxed structures, but still quite comparable because all three Fe potentials were fit to experimental elastic constants.

The formation energies are reproduced within an accuracy of 0.2 eV, and the tetrahedral He interstitial is the most stable in all of the iron matrices. Based on a comparison with the *ab initio* simulation of He migration by Fu and Willaime [5], the new potential accurately describes He interstitial migration. The He migration path from one tetrahedral position to another proceeds in a $\langle 110 \rangle$ direction that does not pass through the octahedral site. The formation energy of a He interstitial at the mid-point of this migration path is denoted by $\text{He}_{i\text{-mid}}$ and is also listed in Table 2. The most stable configuration for two He atoms in a vacancy is found to be a $\langle 100 \rangle$ dumbbell, with a formation energy that is in good agreement with VASP calculations. The new potential somewhat underestimates the formation energy of a He di-interstitial, while overestimating its binding energy by about 0.2 eV. However, this inaccuracy for very closely spaced He atoms should have only a minimal impact on most future applications of the potential. Pure atomic helium clusters are unlikely to be created in significant

numbers because He is easily trapped and strongly bound by vacancies. Overall the potential accurately describes the formation energies before and after relaxation which also indicates its good performance in describing Fe–He forces.

The new Fe–He potential was used to study the properties of He–vacancy clusters at 0 K. The dependence of the binding energy of additional He atoms to a He–vacancy cluster (substitutional He) and the binding energy of a Fe SIA to a He–di-vacancy cluster were investigated as a function of cluster size. The definitions of the binding energies are given in [7]. Periodic boundary conditions were applied to a cubic $10a_0 \times 10a_0 \times 10a_0$ computational cell ($a_0 = \text{bcc iron lattice parameter}$). The atomic coordinates were relaxed using a conjugate-gradient method to zero force at constant volume. The results for He atom and Fe SIA binding

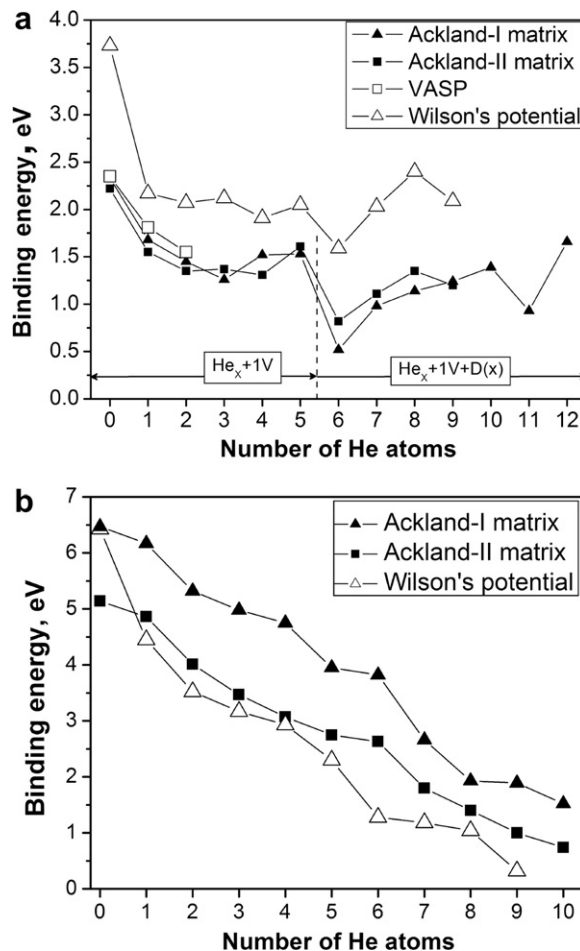


Fig. 1. Binding energy: (a) of additional He atoms to a He–vacancy cluster (substitutional He), and (b) a Fe SIA to a He–di-vacancy cluster versus the number of He atoms in the cluster.

are presented in Fig. 1(a) and (b), respectively, for simulations performed with the Ackland-I [9] and Ackland-II [10] Fe potentials. The results are qualitatively the same with either iron matrix, with a strong atomic relaxation observed around the He–vacancy complex. The binding energies for small He–vacancy clusters calculated from first principles [7] are also shown in Fig. 1(a). The binding energies calculated with the new potential agree with *ab initio* calculations within 0.25 eV. The binding energies obtained from Wilson’s Fe–He pair potential [13] are also presented for comparison. Wilson’s potential systematically overestimates the binding of a He atom to the He–vacancy cluster and underestimates the binding of a Fe SIA.

The binding energy of additional He atoms to the He–vacancy cluster initially decreases and then increases, with a local maximum when a total of six He atoms (five He bound to substitutional He) are involved. In this case, a compact He octahedron is formed with a vacant site at the center. For larger numbers of He atoms, the local dilatations produced by the He–vacancy complex are strong enough to begin displacing iron atoms at the periphery of the cluster. This leads to the decrease in binding energy shown when the sixth He atom (a total of seven He) is added. The notation D(x) in Fig. 1(a) is meant to indicate that significant matrix distortions occur for the larger He contents. An example of these distortions is shown in Fig. 2 for the case of 11 He atoms bound to the He–vacancy cluster. Eight Fe atoms are displaced by $\sim 0.2 a_0$ in approximately $\langle 110 \rangle$ directions to create the extra volume required to accommodate the He. These distributed displacements rather than true Frenkel pair forma-

tion were observed in all the static simulations, and the configuration shown in Fig. 2 suggests the possibility of directly producing Fe interstitial clusters (so-called loop punching) for clusters with greater He content. Dynamic simulations at finite temperature are required to determine if Frenkel pair or interstitial cluster formation is favored.

The strong He binding behavior contrasts with that of a Fe SIA. As shown in Fig. 1(b), the binding energy of an SIA to a He–di–vacancy cluster decreases continuously as the number of He atoms increases. The weaker SIA binding is ultimately a necessary condition for He bubble growth since it favors He–vacancy agglomeration relative to SIA–vacancy recombination for larger He–vacancy clusters.

4. Conclusions

A multi-scale approach has been applied to study He defect properties in iron. An empirical Fe–He potential, consisting of a pair potential and a three-body term, was fitted to *ab initio* data. When used in combination with different iron potentials, it accurately reproduces the energies of a single He defect and small He clusters. The potential was used to study the zero-temperature properties of helium–vacancy clusters. Depending on the size of the cluster, He atoms are bound with an energy that is generally greater than 1.0 eV, while the binding of a Fe self-interstitial to a He–di–vacancy cluster decreases continuously with increasing cluster size. Although the details of the He–vacancy configurations must be potential dependent to some degree in these static simulations, the physical mechanisms are believed to be accurately predicted. The Fe–He potential that has been developed represents a substantial improvement over currently available pair potentials; it is relatively simple, and can be efficiently applied in large-scale molecular dynamics simulations.

Acknowledgements

This research was sponsored by the Division of Materials Sciences and Engineering (Seletskaiya, Osetsky, and Stocks) and the Office of Fusion Energy Sciences (Stoller), US Department of Energy, under contract DE-AC05-00OR22725 with UT-Battelle, LLC.

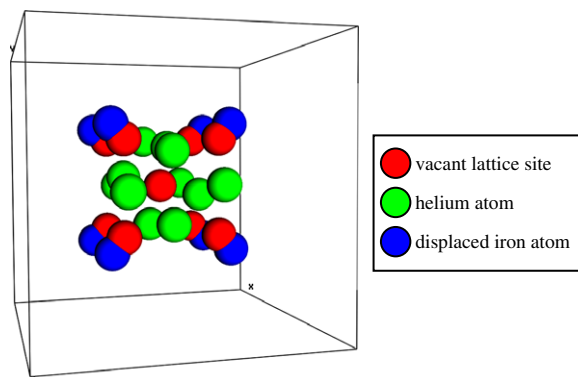


Fig. 2. He–vacancy cluster with a total of 12 He atoms. Initial, true vacancy is shown at center and dilatation-induced defects at the periphery.

References

- [1] R.E. Stoller, J. Nucl. Mater. 174 (1990) 289.
- [2] R. Vassen, H. Trinkaus, P. Jung, Phys. Rev. B 44 (1991) 4206.
- [3] W.D. Wilson, in: M.T. Robinson, F.W. Young (Eds.), Fundamental Aspects of Radiation Damage in Metals, USERDA-CONF-751006-P2, 1975, p. 1025.
- [4] T. Seletskaya, Yuri Osetsky, R.E. Stoller, G.M. Stocks, Phys. Rev. Lett. 94 (2005) 046403.
- [5] C.C. Fu, F. Willaime, Phys. Rev. B 72 (2005) 064117.
- [6] T. Seletskaya, Yu. N Osetsky, R.E. Stoller, G.M. Stocks, in: N.M. Ghoniem (Ed.), Multiscale materials modeling, Proceedings of Second International Conference, University of California, Los Angeles, CA, 2004, p. 545.
- [7] T. Seletskaya, Yu. N. Osetsky, R.E. Stoller, G.M. Stocks, J. Nucl. Mater. 351 (2006) 109.
- [8] M.W. Finnis, J.E. Sinclair, Philos. Mag. A 50 (1984) 45.
- [9] G.J. Ackland, D.J. Bacon, A.F. Calder, T. Harry, Philos. Mag. A 75 (1997) 713.
- [10] G.J. Ackland, M.I. Mendeleev, D.J. Srolovitz, S. Han, A.V. Barashev, J. Phys.: Condens. Matter 16 (2004) S2629.
- [11] M.I. Mendeleev, S. Han, D.J. Srolovitz, G.J. Ackland, D.Y. Sun, M. Asta, Philos. Mag. 83 (2003) 3977.
- [12] R.A. Aziz, A.R. Janzen, M.R. Moldover, Phys. Rev. Lett. 74 (1995) 1586.
- [13] K. Morishita, R. Sugano, B.D. Wirth, T. Diaz de la Rubia, Nucl. Instrum. and Meth. B 202 (2003) 76.